







RESEARCH ARTICLE | APRIL 05 2024

Imperfect phononic crystals work too: The effect of translational and mid-plane symmetry breaking on hypersound propagation

Special Collection: [New Frontiers in Acoustic and Elastic Metamaterials and Metasurfaces](#)

Visnja Babacic ; Marianna Sledzinska ; Thomas Vasileiadis ; Clivia M. Sotomayor Torres ; Bartłomiej Graczykowski  



APL Mater. 12, 041108 (2024)

<https://doi.org/10.1063/5.0189694>



06 June 2024 12:13:41



APL Materials

Special Topic:

Emerging Leaders in Materials Science

Guest Editors: Bo Wang, Marina Leite, Baishakhi Mazumder, Emilie Ringe, Jordi Sort, Ying-Wei Yang

Submit Today!



Imperfect phononic crystals work too: The effect of translational and mid-plane symmetry breaking on hypersound propagation

Cite as: APL Mater. 12, 041108 (2024); doi: 10.1063/5.0189694

Submitted: 30 November 2023 • Accepted: 19 March 2024 •

Published Online: 5 April 2024



Visnja Babacic,¹ Marianna Sledzinska,² Thomas Vasileiadis,¹ Clivia M. Sotomayor Torres,² and Bartlomiej Graczykowski^{1,a)}

AFFILIATIONS

¹ Faculty of Physics, Adam Mickiewicz University, Uniwersytetu Poznanskiego 2, 61-614 Poznan, Poland

² Catalan Institute of Nanoscience and Nanotechnology (ICN2), CSIC and BIST, Campus UAB, Bellaterra, 08193 Barcelona, Spain

Note: This paper is part of the Special Topic on New Frontiers in Acoustic and Elastic Metamaterials and Metasurfaces.

a) Author to whom correspondence should be addressed: bartlomiej.graczykowski@amu.edu.pl

ABSTRACT

Translationally symmetric nanostructures, termed phononic crystals (PnCs), offer control over the propagation of acoustic phonons in the gigahertz (GHz) range for signal-processing applications and thermal management at sub-Kelvin temperatures. In this work, we utilize Brillouin light scattering to investigate the impact of symmetry breaking on GHz phonon propagation in PnCs made of holey silicon nanomembranes. We show that the lattice of thimble-like holes leads to broken mid-plane symmetry and, hence, to anticrossing acoustic band gaps. With the rising level of uncorrelated translational disorder, the phononic effects are gradually suppressed, starting at higher frequencies. Strikingly, the low-frequency partial Bragg bandgap remains robust up to the highest level of disorder.

© 2024 Author(s). All article content, except where otherwise noted, is licensed under a Creative Commons Attribution (CC BY) license (<https://creativecommons.org/licenses/by/4.0/>). <https://doi.org/10.1063/5.0189694>

I. INTRODUCTION

Ordered structures of motives mimicking the atomic structure of natural crystals enable the possibility of controlling electromagnetic, acoustic/elastic, and spin wave propagation in materials called phononic (PnC), photonic (PhC), and magnonic crystals, respectively.^{1–5} The periodicity implicates the appearance of Bragg reflections, Bloch waves, the second-order (in addition to the atomic lattice) Brillouin zones (BZs), zone folding of the dispersion relations, and, in some cases, Bragg gaps where wave transmission is forbidden. In the case of PnCs, when periodic motives are local resonators such as pillars or spheres, hybridization gaps can open besides Bragg gaps.^{1,6–11} The latter are robust to lattice imperfections, but the motives must be uniform. In addition, the geometry (shape and size) of local resonators can tune the position and width of these band gaps.^{8,9,12,13} Photonic and phononic crystals with an ordered lattice are well studied experimentally and theoretically, having the advantage of being easily modeled as they have defined

unit cells with periodic boundary conditions limiting the computational effort. However, from a practical point of view, disorder, roughness, local variations of periodic motifs, lattice constants, and other defects introduced during fabrication are unavoidable. Thus, it is essential to investigate how such imperfections influence the pre-designed properties of those materials and verify if they can lead to unforeseen benefits.

Generally, patterned materials lie between two extremes: from perfect order to uncorrelated disorder. Intermediate states include defective crystals, glass-like structures with short-range order, and quasi-crystalline systems with hyperuniform disorder.¹⁴ The effects of the engineered disorder have already been explored for photonic metamaterials, particularly for structures with hyperuniform disorder.^{14–18} This class of disordered materials is characterized by vanishing density fluctuations at large length scales compared to average distances between the motifs (holes, particles, and inclusions).¹⁹ It has been shown that, contrary to the destruction of photonic band gaps with uncorrelated disorder,²⁰ hyperuniform

structures retain their complete photonic band gaps.^{14–17} Moreover, studies on various highly disordered structures demonstrated photonic or phononic/acoustic Anderson localization,^{21–26} leading to bandgap widening and the emergence of band-tail eigenstates.^{25,27,28} Regarding sub-micrometer feature size PnCs, the lattice disorder was utilized to demonstrate incoherent and coherent phononic effects on nanoscale thermal transport.^{29–35} In addition, recent studies have explored the possibility of increasing thermal conductivity³⁴ or optomechanical coupling^{36,37} with the controlled disorder.

In this work, we investigate the impact of two types of broken symmetry on the gigahertz (GHz) phonon propagation in 2D PnCs made of porous 250 nm thick Si membranes. We employ Brillouin light scattering (BLS) spectroscopy and Finite Element Method (FEM) calculations to explore the modification of the phonon

dispersion relation in 2D PnCs with broken mirror mid-plane and in-plane translational symmetry. Our study reveals the opening of a new type of acoustic stop band due to the anticrossing of symmetric and antisymmetric modes. Furthermore, we show excellent robustness of the low-frequency Bragg gap to high levels of uncorrelated PnC lattice disorder. The results shed new light on imperfect PnC structures and brought nanoscale hypersonic PnCs closer to low-cost applications and large-scale manufacturing.

II. MATERIALS AND METHODS

Solid-air (holey) PnCs were fabricated from silicon-on-insulator (SOI) wafers with device layer thickness $h = 250$ nm using

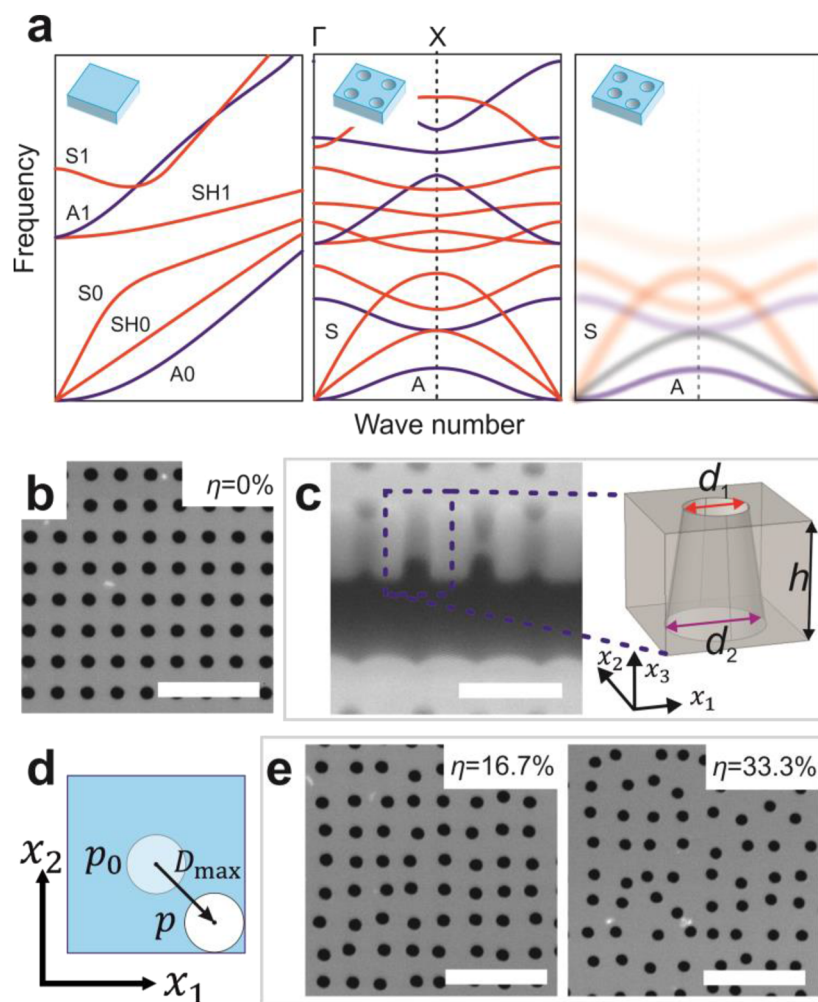


FIG. 1. (a) Schematic phononic band diagrams for plane membrane (left), ordered ($\eta = 0\%$) (center), and disordered ($\eta > 0\%$) 2D PnC (right). (b) SEM top-view image of the ordered PnC made of holes in a 250 nm thick Si membrane. (c) Cross section SEM image of an exemplary sample (left) and the corresponding unit cell of the FEM calculations (right). Symbols d_1 , d_2 , and h denote the diameters of the upper and lower holes and membrane thickness, respectively. (d) Schematic illustration of the random displacement of a hole within a unit cell of the disordered PnC. Symbols p_0 , p , and D_{max} denote the hole position in the ordered lattice, the position after displacement, and the maximum allowed shift distance, respectively. (e) SEM top-view images of exemplary disordered PnCs with the indicated level of disorder, η . The scale bars in (b) and (e) are 1 μm , while in (c) 500 nm.

electron beam lithography (EBL), reactive ion etching (RIE), and subsequent HF vapor under-etching. Figure 1(b) displays the scanning electron microscope (SEM) image of the PnC with an ordered lattice and a lattice constant of $a = 300$ nm. The fabrication process leads to thimble-like holes rather than cylindrical ones and breaks the mid-plane symmetry of the membrane. This case is illustrated in Fig. 1(c) with a cross section SEM image and a schematic illustration of the lattice. The disorder of the PnC lattice was implemented by the random displacements of holes in a quadratic frequency distribution (Fig. S1 in the supplementary material) in x_1 and x_2 -directions, as illustrated in Fig. 1(d). The perturbed hole position along the two in-plane axes is given by $p = p_0 \pm \varepsilon \cdot D_{\max}$. Here, p_0 is the hole position in the ordered lattice, D_{\max} is the maximum allowed shift distance, and ε is a random number between 0 and 1. In the design, we discriminated positions, which could lead to a partial overlap of holes from neighboring unit cells. The level of the lattice disorder was quantified by η , which is given by the ratio of D_{\max} to the lattice constant ($a = 300$ nm) in percentage. The design forbids overlapping holes, which could reduce the porosity (filling factor) globally. Figure 1(e) displays SEM top-view images of two exemplary PnCs differing in the level of the in-plane translational disorder, while Table S1 (the supplementary material) summarizes the values of the parameters D_{\max} and η for all the samples.

A. Brillouin light scattering

Brillouin light scattering (BLS) measurements were performed in the backscattering geometry (Fig. S2 in the supplementary material) with a single-mode laser incident light source (Spectra-Physics, Excelsior 300) operating at the wavelength $\lambda = 532$ nm and power adjusted to less than 5 mW. The measurements were performed in the p - p polarization configuration regarding incident-scattered light, where p denotes the polarization parallel to the sagittal plane (plane of incidence). The incident light of p polarization, set by placing a half-wave ($\lambda/2$) plate on its path, was partially reflected from a pellicle beamsplitter (BS, R:T, 8:92) and then focused on the sample by a microscope objective with $50\times$ magnification, working distance (WD) = 22 mm, and numerical aperture (NA) = 0.45. The sample holder was placed on a rotation stage to select the incident angle θ . The same objective was used to collect the light scattered from the sample. The magnitude of the scattering wave vector was set by changing the scattering angle and following the formula $q = 4\pi \sin \theta / \lambda$. The scattered light was analyzed with a tandem-type Fabry-Perot interferometer (Table Stable Ltd. Vibration Isolation and JRS Optical Instruments).

B. Finite element method

In order to calculate the dispersion relations of the ordered PnCs, we used the Finite Element Method (FEM, COMSOL Multiphysics). The calculations were performed in the frequency domain by searching for undamped eigenfrequencies and with Bloch periodic boundary conditions that allow sweeping the phonon wavevector across the BZ. Based on the SEM images, the model's unit cell length and thickness [Figs. 1(c) and S3(a) in the supplementary material] were $a = 300$ nm and $h = 250$ nm, respectively. The thimble-like holes had diameters of $d_1 = 135$ nm and $d_2 = 210$ nm. In addition, we performed comparative FEM modeling of PnCs preserving the mid-plane mirror symmetry, i.e., made of the lattice

of cylindrical holes. In this case, the cylinder diameter was set to $d = \sqrt{(d_1^2 + d_1 d_2 + d_2^2)/3} \cong 174$ nm, keeping the same porosity of the structure in this way.

Eigenfrequencies, given as $f = \omega/2\pi$, where ω is the angular frequency, were calculated from the elastic wave equation,

$$-\rho \omega^2 u_i = \frac{\partial \sigma_{ij}}{\partial x_j}, \quad (1)$$

where ρ is the mass density, u_i are components of the displacement vector, and σ_{ij} (summation for $i, j = 1, 2, 3$) is the Cauchy stress tensor. This stress tensor is defined by Hooke's law as $\sigma_{ij} = C_{ijkl} \varepsilon_{kl}$, where ε_{kl} is the strain tensor, and C_{ijkl} is an order elastic tensor ($i, j, k, l = 1, 2, 3$) that can be expressed as a 6×6 matrix in the Voigt notation, C_{KL} ($ij \rightarrow K, kl \rightarrow L$; $K, L = 1, 2, \dots, 6$). Since silicon has cubic symmetry, its elastic properties are defined by three non-zero independent elastic constants, namely, $C_{11} = 165.7$ GPa, $C_{12} = 63.9$ GPa, and $C_{44} = 79.9$ GPa. Considering the orientation of the unit cell following the crystallographic orientation of the sample, the elastic properties were defined with elastic constants after a rotation of 45° around the x_3 axis: $C'_{11} = C'_{22} = 194.7$ GPa, $C'_{33} = C_{11}$, $C'_{44} = C'_{55} = C_{44}$, $C'_{66} = 50.9$ GPa, $C'_{12} = 34.9$ GPa, and $C'_{13} = C'_{23} = C_{12}$.³⁸ The mass density was $\rho = 2331$ kg/m³.³⁸

To obtain the dispersion relation in the form of $f(q)$, we calculated frequencies of eigenmodes with q swept with 500 equally spaced steps in the $\Gamma - X$ direction ($0 - 10.47 \mu\text{m}^{-1}$). To distinguish symmetric and antisymmetric modes, we calculate the surface integral,

$$\chi_Z = \frac{1}{S} \int_S \frac{u_3|_{x_3=0}}{u_3|_{x_3=h}} dS, \quad (2)$$

where the integral is normalized with the upper (or lower) surface S of the unit cell. The mode-dependent parameter χ_Z gives +1 or -1 for antisymmetric or symmetric modes, respectively. In the case of conical holes, the broken mid-plane symmetry partially lifts the distinction between symmetric and antisymmetric modes, and the $|\chi_Z|$ is not properly normalized (for some modes, $|\chi_Z| > 1$). However, certain parts of the band structure retain the symmetric/antisymmetric character even for conical holes, such as the three lowest branches in the long-wavelength limit. Finally, we also employed FEM to calculate the dispersion relation for the effective medium of different porosities when compared to the pristine silicone membrane. In this simulation, we assumed a transversely isotropic material with elastic constants for bulk silicon.

III. RESULTS AND DISCUSSION

A. Influence of broken mid-plane symmetry on the band structure

In pristine membranes, 1D confinement results in the appearance of the family of symmetric (S), antisymmetric (A), and shear horizontal (SH) Lamb waves, as illustrated in Fig. 1(a). Introducing the ordered lattice of holes leads to the appearance of Bloch waves and, hence, the formation of the second-order BZs and band folding at the edges of the BZs. This can lead to the Bragg gap opening for all branches (full) or specific symmetries of the modes (A, S, or SH), as illustrated in Fig. 1(a). In the case of an imperfect lattice, the

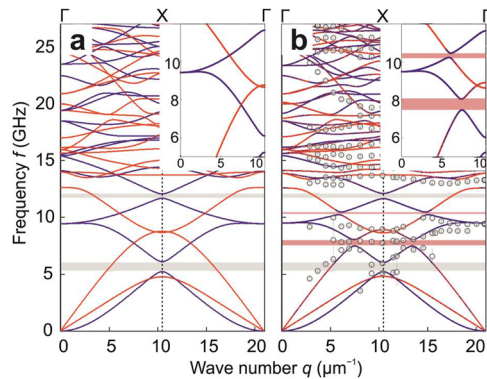


FIG. 2. Calculated phononic dispersion in the ΓX direction for PnC with (a) cylindrical holes and (b) truncated cone holes. The band gaps are indicated by the shaded area. Blue and red lines denote antisymmetric A and symmetric S modes, respectively. Insets in (a) and (b) show zoom-in depicting the transition from crossing to avoided crossing of A and S branches. Circles in (b) denote experimental BLS data.

phonon coherence gradually vanishes while the disorder η increases. First, this leads to the BZ edges blurring and vanishing of the zone folding. A sufficient level of non-correlated disorder results in the phonon dispersion of a randomly porous membrane resembling an effective medium.

Before discussing the effect of symmetry-lowering in 2D PnCs, we considered an ideal case of PnC maintaining translational and mid-plane mirror symmetries as a reference. Figure 2(a) demonstrates the calculated dispersion for the ΓX direction of the PnC with an ordered lattice and cylindrical holes. Here, the branches corresponding to S and A modes are denoted with red and blue lines, respectively. In the case of an ideal PnC, both A and S modes may contain the SH component of the displacement. However, A and S modes are orthogonal and do not interact, i.e., their branches can cross in the band diagram. In Fig. 2(a), we notice only two partial Bragg band gaps for the antisymmetric modes at the X point of BZ, indicated with shading.

However, the experimental dispersion relation plotted in Fig. 2(b) (circles) did not match that of the ideal case of PnC described above and depicted in Fig. 2(a). Only after adjusting the hole shape to the truncated cone (thimble), as in Fig. 1(c), do we obtain good agreement between the calculated dispersion relation for the ΓX direction and the BLS data [Fig. 2(b)]. The calculated dispersions for XM and MF directions are shown in the supplementary material (Fig. S4). Here, we focus the discussion on the ΓX direction, and we identify different band gaps in PnC with thimble-like holes. Partial Bragg gaps at the X point of BZ remained unaffected compared to PnC with cylindrical holes. More interestingly, the dispersion of PnC in the thimble-like holes revealed two full band gaps denoted by shaded areas in Fig. 2(b). They are centered at about 7.75 and 10.35 GHz, with widths of about 0.50 and 0.20 GHz, respectively. This type of acoustic stop-band was predicted theoretically for one-dimensional PnCs³⁹ and can be attributed to the anticrossing of branches due to the broken mid-plane symmetry of PnC. In this case, modes can no longer be separated into purely antisymmetric

and symmetric, as illustrated in Fig. 2(b). Consequently, the quasi-antisymmetric and quasi-symmetric modes can interact, enabling the gap to open at arbitrary wavenumbers. This feature makes the anticrossing bandgaps similar to the local resonance gaps, although there is no resonant element in the structure. This also emphasizes their difference with the Bragg gaps localized at the high symmetry points of BZ. The insets in Fig. 2 display zoom-in fragments of the band diagrams that depict the transition of the dispersion relation from the ideal (cylindrical hole) to the real (thimble-like hole) structure. Here, FEM displacement fields show that mid-plane symmetry breaking is localizing the elastic energy either on the upper or lower membrane surface, and this localization leads to the bandgap opening. Our calculations also show the possibility of tuning the width of avoided crossing band gaps by the degree to which the PnC is away from mid-plane symmetry. The influence of the cone angle on these band gaps is shown in Fig. S5. In perspective, this type of tunable bandgap could be found in 1D, 2D, and 3D PnCs with different asymmetric motives that break their mirror symmetry.

B. Broken translational in-plane symmetry

We examined nine samples to reveal the effect of the translational disorder in 2D PnCs on the phononic dispersion relation, with a particular focus on the band gaps. The samples had thimble-like holes and the same porosity, although they differed in the level of pre-designed disorder, η ranging from 0% to 33.3%. Figure 3 displays experimental band diagrams obtained for two extreme cases of the lattice disorder. Here, BLS data are displayed as a color map showing the scattered light intensity and compared to band diagrams calculated by FEM. As we can notice, BLS does not probe all the phononic modes. In general, in this particular experimental configuration, the BLS-active modes are those of out-of-plane displacement due to the dominant role of the surface-ripple (moving interface) mechanism. At first glance, comparing the band diagrams in Fig. 3, we notice a significant decrease in the number of branches due to the disorder.

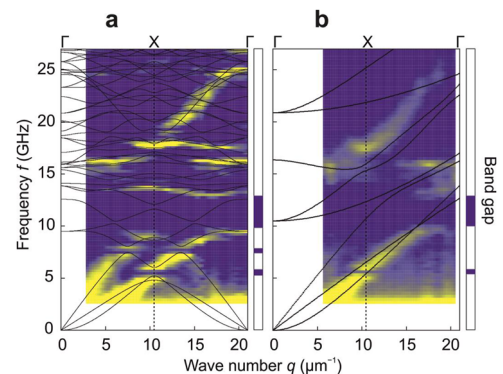


FIG. 3. Experimental phononic dispersion relation in ΓX direction for the (a) ordered PnC and (b) PnC with the highest considered level of disorder, $\eta = 33.3\%$. In (a), the color plot and lines denote experimental data and calculated dispersion, respectively. In (b), the color plot and lines denote experimental data and calculated dispersion for the effective medium (the plane membrane of a corresponding porosity). Band gaps of importance are indicated on the right side of each panel.

On the other hand, the dispersion of the disordered PnC does not match the predictions of the FEM model for the effective medium and reveals the remaining features of the ordered PnC. In particular, the low-frequency partial (quasi-antisymmetric) bandgap is preserved. In addition, two flat branches at about 12–15 GHz are a common feature of ordered and disordered systems, despite not being predicted for the latter in the effective medium model. This feature is somewhat surprising, considering that the literature reports the strong influence of disorder on the Bragg gap in photonic crystals.^{40,41} Contrarily, the preservation of band gaps in PnCs and PnCs with correlated disorders was previously reported for hyperuniform structures.^{14,16,42} However, this is not the case in our study, as the design and fabrication were based on the uncorrelated disorder and not aimed at hyperuniform PnCs.

To shed more light on the lattice order-disorder transition and its consequences for phonon propagation, we examined all nine PnCs with gradually changing levels of disorder. In this case, we probed BLS spectra only at the scattering angle set to $\theta = 26^\circ$, which corresponds to the X high symmetry point of BZ. Nevertheless, we did not discriminate the scattered light cone by any additional aperture before the spectrometer in this experiment. Therefore, the scattered wave vector was ill-defined, spanning a broad area of the BZ around the X-point. In this way, the recorded spectra resembled the phononic Density of States (DOSs), with singularities and

gaps being fingerprints of the coherent effects in PnCs. For instance, the BLS spectrum in Fig. 4(a) shows sharp peaks corresponding to singularities typical for the ordered sample ($\eta = 0\%$). Increasing the disorder leads to reduced coherence, as evidenced by the disappearance of peaks in the spectra starting at higher frequencies. However, some peaks remain even at the highest level of disorder, especially in the low-frequency region below about 25 GHz. Figure 4(b) displays the SEM and corresponding fast Fourier transform (FFT) images for the exemplary samples with different levels of disorder. The FFT of the ordered sample shows a crystalline structure characterized by translational order. The increase in the disorder to 6.7% leads to a structure that can be classified as a defective crystal. Furthermore, some crystallinity prevails at 13.3%, but it is finally lost at 20% of the disorder. Therefore, we can see that for the level of disorder $\geq 20\%$, our samples are neither crystalline nor hyperuniform; they exhibit uncorrelated disorder. Figure 4(c) displayed BLS spectra gathered as a colormap limited to the low-frequency spectral range. Interestingly, the partial Bragg gap is present in all the samples, even for the highest level of uncorrelated disorder. The increase in disorder impacts the width of the bandgap, which slightly decreases and blueshifts. In addition, we notice that the influence of disorder is more substantial on the anticrossing bandgap. Nevertheless, it prevails for relatively high disorders, i.e., ($\eta = 20\%$).

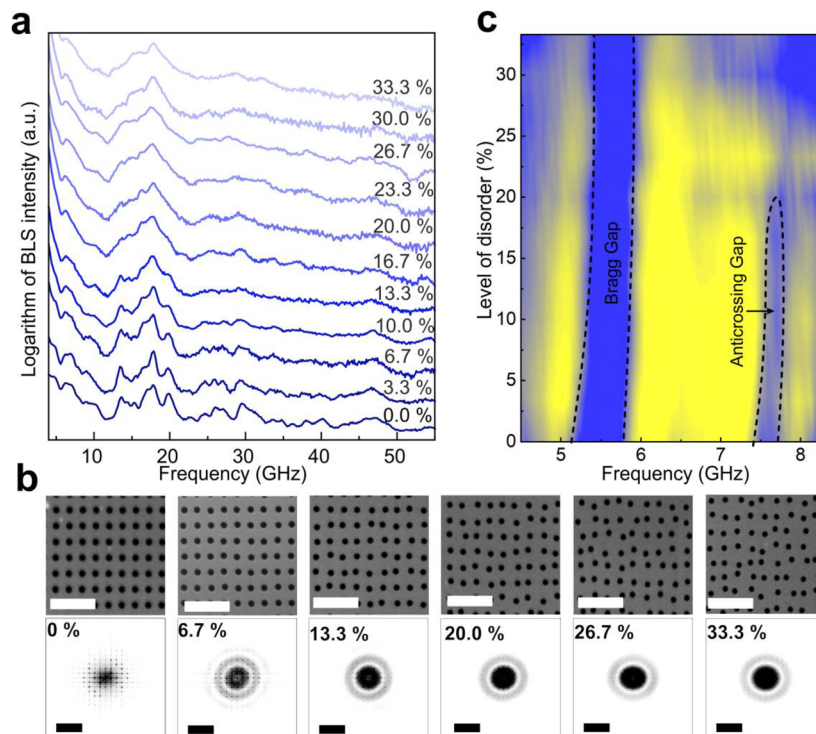


FIG. 4. (a) Broad wavenumber experimental BLS spectra obtained at $\theta = 26^\circ$ resembling DOS obtained for PnCs with increasing levels of disorder. (b) SEM images (top) and corresponding fast Fourier transform images (bottom) of exemplary PnCs with different levels of disorder η . Scale bars are $1\ \mu\text{m}$ and $0.1\ \mu\text{m}^{-1}$, respectively. (c) Measured (BLS spectra map) evolution of the partial Bragg gap and the anticrossing gap with the disorder. Dashed lines indicate the guide to the eye for the bandgap.

IV. CONCLUSIONS

In this work, we presented an experimental study of the impact of two types of structural imperfections on GHz phonon propagation in 2D PnCs made of porous Si nanomembranes. We showed that the periodic perforation of the membrane by thimble-like holes breaks its mid-plane mirror symmetry. Consequently, it leads to a forbidden propagation band due to anticrossing. This sort of phononic bandgap has been demonstrated theoretically before. However, it has not been reported in any experimental work. In contrast to the Bragg gaps, the anticrossing gaps appear away from the high-symmetry points. Notably, breaking the mirror symmetry provides new geometrical means for the tunability of PnCs by the holes' cross-sectional shape in addition to their size and periodic arrangement.

The second type of structural imperfection of PnCs, i.e., pre-designed perturbation of the square lattice, was studied on nine samples, differing only in the level of uncorrelated disorder. Interestingly, the phononic dispersion relation of the most disordered PnC ($\eta = 33.3\%$) did not transform into the dispersion of an effective medium, and even more, it kept some features of the ordered PnC. While the increased disorder is expected to destroy phonon coherence starting at higher frequencies, the low-frequency spectral features are more robust. Foremost, the low-frequency Bragg bandgap was preserved despite the high uncorrelated disorder, while the anticrossing gap was maintained up to $\eta = 20\%$ disorder.

Our findings showed that the structural imperfections do not spoil selective sound propagation via Bragg gaps and can provide a new PnC tuning scheme that is also robust to some extent of disorder via anticrossing gaps. Thus, PnCs with uncorrelated disordered lattices due to pre-design or fabrication imperfections can be utilized in the free-form acoustic waveguides. Furthermore, the results presented can have implications in low-temperature nanoscale thermal transport studies where disordered PnCs are assumed to be model systems with no coherent effect on phononic heat propagation.^{43,44} Finally, we demonstrated the possibility of experimental studies of phononic properties in highly disordered PnCs, which, to date, have been incredibly challenging for numerical models. Similar experimental studies can be carried out to study highly disordered systems with a focus on acoustic Anderson localization, phononic quasicrystals, moiré patterns, or Fibonacci structures.

SUPPLEMENTARY MATERIAL

Histogram of the holes' random distribution. Maximum holes' shift, corresponding disorder level η , and porosity. Schematic illustration of Brillouin light scattering geometry and samples' design. Calculated phonon dispersion of ordered PnC.

ACKNOWLEDGMENTS

The work was supported by the National Science Center of Poland (NCN) by OPUS Grant No. 2021/41/B/ST5/03038 and the National Center for Research and Development by Grant No. EIG CONCERT-JAPAN/9/91/PETITE/2023. The ICN2 was supported by the Severo Ochoa Centres of Excellence programme [SEV-2017-0706] and is currently supported by the Severo Ochoa Centres of Excellence programme, Grant CEX2021-001214-S, both

funded by MCIN/AEI/10.13039.501100011033 and the CERCA Programme/Generalitat de Catalunya. M.S. acknowledges support from the MCIN/AEI grant PETITE (Grant No. PCI2023-143399)

AUTHOR DECLARATIONS

Conflict of Interest

The authors declare that they have no known competing financial interests or personal relationships that could have appeared to influence the work reported in this paper.

Author Contributions

Visnja Babacic: Data curation (equal); Formal analysis (equal); Investigation (equal); Validation (equal); Visualization (equal); Writing – original draft (equal); Writing – review & editing (equal). **Marianna Sledzinska:** Investigation (equal); Methodology (equal); Resources (equal); Software (equal); Visualization (equal). **Thomas Vasileiadis:** Formal analysis (equal); Investigation (equal). **Clivia M. Sotomayor Torres:** Methodology (equal); Project administration (equal); Resources (equal). **Bartłomiej Graczykowski:** Conceptualization (equal); Data curation (equal); Formal analysis (equal); Funding acquisition (equal); Investigation (equal); Methodology (equal); Project administration (equal); Resources (equal); Software (equal); Supervision (equal); Validation (equal); Visualization (equal); Writing – original draft (equal); Writing – review & editing (equal).

DATA AVAILABILITY

The data that support the findings of this study are available from the corresponding author upon reasonable request.

REFERENCES

- T. Vasileiadis, J. Varghese, V. Babacic, J. Gomis-Bresco, D. Navarro Urrios, and B. Graczykowski, "Progress and perspectives on phononic crystals," *J. Appl. Phys.* **129**, 160901 (2021).
- C. M. Soukoulis, "North atlantic treaty organization," *Photonic Band Gap Materials* (Kluwer Academic Publishers, Dordrecht, Boston, 1996).
- A. V. Chumak, A. A. Serga, and B. Hillebrands, "Magnonic crystals for data processing," *J. Phys. D: Appl. Phys.* **50**, 244001 (2017).
- Z. K. Wang, V. L. Zhang, H. S. Lim, S. C. Ng, M. H. Kuok, S. Jain, and A. O. Adeyeye, "Nanostructured magnonic crystals with size-tunable bandgaps," *ACS Nano* **4**, 643–648 (2010).
- J. D. Joannopoulos, P. R. Villeneuve, and S. Fan, "Photonic crystals: Putting a new twist on light," *Nature* **386**, 143–149 (1997).
- B. Graczykowski, N. Vogel, K. Bley, H.-J. Butt, and G. Fytas, "Multiband hyper-sound filtering in two-dimensional colloidal crystals: Adhesion, resonances, and periodicity," *Nano Lett.* **20**, 1883–1889 (2020).
- Y. Achaoui, A. Khelif, S. Benchabane, L. Robert, and V. Laude, "Experimental observation of locally-resonant and Bragg band gaps for surface guided waves in a phononic crystal of pillars," *Phys. Rev. B* **83**, 104201 (2011).
- M. Sledzinska, B. Graczykowski, J. Maire, E. Chavez-Angel, C. M. Sotomayor-Torres, and F. Alzina, "2D phononic crystals: Progress and prospects in hypersound and thermal transport engineering," *Adv. Funct. Mater.* **30**, 1904434 (2020).
- Y. Pennec, J. O. Vasseur, B. Djafari-Rouhani, L. Dobrzyński, and P. A. Deymier, "Two-dimensional phononic crystals: Examples and applications," *Surf. Sci. Rep.* **65**, 229–291 (2010).

- ¹⁰Z. Liu, X. Zhang, Y. Mao, Y. Y. Zhu, Z. Yang, C. T. Chan, and P. Sheng, “Locally resonant sonic materials,” *Science* **289**, 1734–1736 (2000).
- ¹¹T. Still, W. Cheng, M. Retsch, R. Sainidou, J. Wang, U. Jonas, N. Stefanou, and G. Fytas, “Simultaneous occurrence of structure-directed and particle-resonance-induced phononic gaps in colloidal films,” *Phys. Rev. Lett.* **100**, 194301 (2008).
- ¹²R. Pourabolghasem, R. Dehghannasiri, A. A. Eftekhari, and A. Adibi, “Waveguiding effect in the gigahertz frequency range in pillar-based phononic-crystal slabs,” *Phys. Rev. Appl.* **9**, 014013 (2018).
- ¹³E. Alonso-Redondo, M. Schmitt, Z. Urbach, C. M. Hui, R. Sainidou, P. Rembert, K. Matyjaszewski, M. R. Bockstaller, and G. Fytas, “A new class of tunable hyper-sonic phononic crystals based on polymer-tethered colloids,” *Nat. Commun.* **6**, 8309 (2015).
- ¹⁴S. Yu, C.-W. Qiu, Y. Chong, S. Torquato, and N. Park, “Engineered disorder in photonics,” *Nat. Rev. Mater.* **6**, 226–243 (2020).
- ¹⁵M. Florescu, S. Torquato, and P. J. Steinhardt, “Designer disordered materials with large, complete photonic band gaps,” *Proc. Natl. Acad. Sci. U. S. A.* **106**, 20658–20663 (2009).
- ¹⁶J. Ricouvier, P. Tabeling, and P. Yazhghur, “Foam as a self-assembling amorphous photonic band gap material,” *Proc. Natl. Acad. Sci. U. S. A.* **116**, 9202–9207 (2019).
- ¹⁷W. Man, M. Florescu, E. P. Williamson, Y. He, S. R. Hashemizad, B. Y. C. Leung, D. R. Liner, S. Torquato, P. M. Chaikin, and P. J. Steinhardt, “Isotropic band gaps and freeform waveguides observed in hyperuniform disordered photonic solids,” *Proc. Natl. Acad. Sci. U. S. A.* **110**, 15886–15891 (2013).
- ¹⁸P. M. Piechulla, B. Fuhrmann, E. Slivina, C. Rockstuhl, R. B. Wehrspohn, and A. N. Sprafke, “Tailored light scattering through hyperuniform disorder in self-organized arrays of high-index nanodisks,” *Adv. Opt. Mater.* **9**, 2100186 (2021).
- ¹⁹R. Dreyfus, Y. Xu, T. Still, L. A. Hough, A. G. Yodh, and S. Torquato, “Diagnosing hyperuniformity in two-dimensional, disordered, jammed packings of soft spheres,” *Phys. Rev. E* **91**, 012302 (2015).
- ²⁰Z.-Y. Li and Z.-Q. Zhang, “Fragility of photonic band gaps in inverse-opal photonic crystals,” *Phys. Rev. B* **62**, 1516–1519 (2000).
- ²¹P. D. García, R. Sapienza, C. Toninelli, C. López, and D. S. Wiersma, “Photonic crystals with controlled disorder,” *Phys. Rev. A* **84**, 023813 (2011).
- ²²L. S. Froufe-Pérez, M. Engel, J. J. Sáenz, and F. Scheffold, “Band gap formation and Anderson localization in disordered photonic materials with structural correlations,” *Proc. Natl. Acad. Sci. U. S. A.* **114**, 9570–9574 (2017).
- ²³T. Schwartz, G. Bartal, S. Fishman, and M. Segev, “Transport and Anderson localization in disordered two-dimensional photonic lattices,” *Nature* **446**, 52–55 (2007).
- ²⁴J. P. Vasco and S. Hughes, “Anderson localization in disordered LN photonic crystal slab cavities,” *ACS Photonics* **5**, 1262–1272 (2018).
- ²⁵R. Sainidou, N. Stefanou, and A. Modinos, “Widening of phononic transmission gaps via Anderson localization,” *Phys. Rev. Lett.* **94**, 205503 (2005).
- ²⁶D. Guzman-Silva, M. Heinrich, T. Biesenhal, Y. V. Kartashov, and A. Szameit, “Experimental study of the interplay between dynamic localization and Anderson localization,” *Opt. Lett.* **45**, 415 (2020).
- ²⁷M. Lee, J. Lee, S. Kim, S. Callard, C. Seassal, and H. Jeon, “Anderson localizations and photonic band-tail states observed in compositionally disordered platform,” *Sci. Adv.* **4**, e1602796 (2018).
- ²⁸G. Gkantounis, T. Amoah, and M. Florescu, “Hyperuniform disordered phononic structures,” *Phys. Rev. B* **95**, 094120 (2017).
- ²⁹S. Hu, Z. Zhang, P. Jiang, W. Ren, C. Yu, J. Shiomi, and J. Chen, “Disorder limits the coherent phonon transport in two-dimensional phononic crystal structures,” *Nanoscale* **11**, 11839–11846 (2019).
- ³⁰S. Hu, Z. Zhang, P. Jiang, J. Chen, S. Volz, M. Nomura, and B. Li, “Randomness-induced phonon localization in graphene heat conduction,” *J. Phys. Chem. Lett.* **9**, 3959–3968 (2018).
- ³¹D. Chakraborty, S. Foster, and N. Neophytou, “Monte Carlo phonon transport simulations in hierarchically disordered silicon nanostructures,” *Phys. Rev. B* **98**, 115435 (2018).
- ³²G. Xie, Z. Ju, K. Zhou, X. Wei, Z. Guo, Y. Cai, and G. Zhang, “Ultra-low thermal conductivity of two-dimensional phononic crystals in the incoherent regime,” *npj Comput. Mater.* **4**, 21 (2018).
- ³³T. Juntunen, O. Vänskä, and I. Tittonen, “Anderson localization quenches thermal transport in aperiodic superlattices,” *Phys. Rev. Lett.* **122**, 105901 (2019).
- ³⁴H. Wei, H. Bao, and X. Ruan, “Genetic algorithm-driven discovery of unexpected thermal conductivity enhancement by disorder,” *Nano Energy* **71**, 104619 (2020).
- ³⁵H. Wei, Y. Hu, and H. Bao, “Influence of point defects and multiscale pores on the different phonon transport regimes,” *Commun. Mater.* **4**, 3–9 (2023).
- ³⁶P. D. García, R. Bericat-Vadell, G. Arregui, D. Navarro-Urrios, M. Colom-bano, F. Alzina, and C. M. Sotomayor-Torres, “Optomechanical coupling in the Anderson-localization regime,” *Phys. Rev. B* **95**, 115129 (2017).
- ³⁷G. Arregui, N. D. Lanzillotti-Kimura, C. M. Sotomayor-Torres, and P. D. García, “Anderson photon-phonon colocalization in certain random superlattices,” *Phys. Rev. Lett.* **122**, 043903 (2019).
- ³⁸B. Graczykowski, M. Sledzinska, F. Alzina, J. Gomis-Bresco, J. S. Reparaz, M. R. Wagner, and C. M. Sotomayor Torres, “Phonon dispersion in hyper-sonic two-dimensional phononic crystal membranes,” *Phys. Rev. B* **91**, 075414 (2015).
- ³⁹Z. Hou and B. M. Assouar, “Opening a band gap in the free phononic crystal thin plate with or without a mirror plane,” *J. Phys. D: Appl. Phys.* **41**, 215102 (2008).
- ⁴⁰C. Liu, M. V. Rybin, P. Mao, S. Zhang, and Y. Kivshar, “Disorder-Immune photonics based on mie-resonant dielectric metamaterials,” *Phys. Rev. Lett.* **123**, 163901 (2019).
- ⁴¹J. Lian, J.-X. Fu, L. Gan, and Z.-Y. Li, “Robust and disorder-immune magnetically tunable one-way waveguides in a gyromagnetic photonic crystal,” *Phys. Rev. B* **85**, 125108 (2012).
- ⁴²M. M. Milošević, W. Man, G. Nahal, P. J. Steinhardt, S. Torquato, P. M. Chaikin, T. Amoah, B. Yu, R. A. Mullen, and M. Florescu, “Hyperuniform disordered waveguides and devices for near infrared silicon photonics,” *Sci. Rep.* **9**, 20338 (2019).
- ⁴³R. Anufriev, D. Otori, Y. Wu, R. Yanagisawa, L. Jalabert, S. Samukawa, and M. Nomura, “Impact of nanopillars on phonon dispersion and thermal conductivity of silicon membranes,” *Nanoscale* **15**, 2248–2253 (2023).
- ⁴⁴R. Anufriev, Y. Wu, J. Ordóñez-Miranda, and M. Nomura, “Nanoscale limit of the thermal conductivity in crystalline silicon carbide membranes, nanowires, and phononic crystals,” *NPG Asia Mater.* **14**, 35 (2022).